

# Film Cooling and Hub Disk Leakage Flow Experiments in a Fully Rotating HP Turbine Stage

PAU, M., DE LA LOMA, A., PANIAGUA, G., DELHAYE, D.

Turbomachinery and Propulsion Department

Von Karman Institute for Fluid Dynamics

Chaussée de Waterloo 72, B1640 – Sint Genesius Rode

BELGIUM

[pau@vki.ac.be](mailto:pau@vki.ac.be) [www.vki.ac.be](http://www.vki.ac.be)

*Abstract:* - This paper describes the experimental methodology, test conditions, and uncertainty analysis concerning a novel rim seal film cooling experiments on a fully rotating HP transonic turbine stage under engine representative conditions. A complex secondary air system has been designed in order to feed the cooled turbine. The rotor blade has been heavily instrumented at the platform, 7% and 15% of the blade height with fast response pressure sensors and double-layer thin film gauges, allowing a complete aero-thermal characterization of the flow field. The hub disk leakage and platform cooling blowing ratios have been varied independently in order to assess their impact individually. Furthermore, tests have been performed at two different rotational speeds. The presented study should help designers improve the protection of the rotor platform and minimize the amount of coolant used.

*Key-Words:* - Gas turbine, leakage flows, film cooling.

## 1. Introduction

An increase of the specific work and cycle efficiency of gas turbines can be achieved through higher turbine inlet temperatures. Ensuring an adequate blade life at these harsh temperatures requires efficient cooling methods. In high pressure turbine stages cold air is usually ejected from the cavity which exists between the stator rim and the rotor disk, to avoid hot gas injection into the wheelspace interface.

Turbine designers should consider three important issues when designing a high pressure turbine stage with active wheelspace cooling, as described by McLean et al. (2001):

- 1) The coolant temperature should be set to maintain the wheelspace temperature below the critical material temperature.
- 2) The coolant flow rates should be adjusted to minimize the aerodynamic losses due to mixing with the mainstream flow as well as the windage losses due to the rotational drag within the same wheelspace cavity.
- 3) Purge flow effects on the rotor endwall heat transfer should be taken into account.

The complex flowfield inside the wheelspace cavity is described by Phadke and Owen (1988), Ko and Rhode (1992), and Laroche et al. (1999), neglecting the interaction between the purge flow and the mainstream flow. Pfau et al. (2001), Anker et al. (2002), Hunter and Manawaring (2000), Rosic et al. (2006) have investigated the cavity-mainstream interaction with the leakage flow being

extracted from the mainstream. Several research groups have been investigating the effects of rotating and stationary pressure asymmetries for the last decade (Bohn et al., 1995, Roy et al., 2001, Gentilhomme et al., 2003, Cao et al., 2003). At engine conditions, circumferential pressure asymmetries are the primary cause of ingestion. All the aforementioned authors concluded that purge flow significantly affects the main gas stream despite injecting only a fraction of the mainstream mass flow. Marini and Girgis (2007) investigated the efficiency sensitivity to cavity flows using CFD with two platform shapes. The broad literature attest the importance of purge flows to turbine design.

Platform film cooling investigations have been predominantly conducted on linear vane cascades. One of the earliest studies on platform film cooling was carried out by Blair (1974) using an upstream slot in a large-scale turbine vane passage. Harasgama and Burton (1992) conducted heat transfer and aerodynamic measurements in an annular cascade fitted with vanes under engine-representative flow conditions. Their results show that film cooling reduced the Nusselt number on the suction side by about 50 %, suggesting that the coolant was convected towards that region by the passage vortex. Friedrichs et al. (1996) described in detail the aerodynamic aspects of platform film cooling using the ammonia and diazo technique. Based on the cooling effectiveness distributions measured in a large scale low-speed turbine

cascade, it was concluded that the film cooling traces moved towards the suction side. The coolant film was found to be eroded by the secondary flows, being pushed towards the suction side, thus leading to an increase of aerodynamic losses due to the mixing process.

Experimental studies on film cooling and heat transfer performed on a rotating turbine platform are scarce in the open literature, primarily due to the difficulties in instrumenting rotating parts. Dring et al. (1980) investigated film cooling performance in a low speed rotating facility, showing that the film coolant experienced only a small radial displacement on the suction side, similarly to flat plate results. On the pressure side, the film coolant trace followed an important radial displacement towards the blade tip. Heat transfer effectiveness distributions along the blade span for rotating turbine blades were obtained by Takeishi et al. (1992) and Abhari and Epstein (1994) using respectively gas chromatography and thin film heat flux gauges. Blair (1994) also studied the heat transfer on the pressure and suction sides as well as on the hub platform for a rotating turbine model. Enhanced heat transfer was observed on the platform due to the effect of the secondary flows. Recently, Ahn et al. (2004) investigated film cooling effectiveness on the leading edge of a rotating blade using pressure sensitive paint. The rotational speed was found to alter significantly the film coolant traces on the blade leading edge.

Platform film cooling in a revolving rotor has yet never been tackled in the open literature and is explored in the present study. The present work aims to quantify and understand the influence of stator-rim purge flow and of rotor-platform film cooling on the aero thermal flow field in a transonic high pressure turbine. The acquired data will help to validate advanced CFD models, and the results analysis will contribute to comprehend the flow interactions occurring in cooled transonic turbines. The tests were carried out in a full stage under engine-representative conditions. The VKI CT3 multipurpose turbine research facility was equipped with new blades and modified to accommodate the present film cooling research.

In the present work turbine test rig, coolant supply system, advanced instrumentation and data processing techniques are first described. Secondly the operation of the facility, test conditions and coolant flow features are presented and commented. Finally the measured coolant flow rate are discussed.

## 2. Nomenclature

$C$	Chord [m]
HBL	Hub disk leakage
$Br$	Blowing ratio
$Dr$	Density ratio
$M$	Mach number
$M$	Momentum ratio
$P$	Pressure [bar]
$Re$	Reynolds number $\rho \cdot V \cdot C / \mu$
$S$	Curvilinear abscissa [m]
$T$	Temperature [K]
$t$	Time [s]
$x$	Axial distance [m]

### Subscripts

0	Total conditions
1	Stator inlet
2	Stator outlet, rotor inlet
3	Rotor outlet
$r$	Relative conditions
$ax$	axial
h	hub
is	isentropic

## 3. Experimental apparatus and method

### 3.1. Turbine test rig

The measurements have been performed in the compression tube turbine test rig CT3 at the Von Karman Institute. The operation cycle of the rig is fully described by Dénos and Paniagua (2005).

Main stream	Engine	Rig
Reynolds	$10^6$	$10^6$
$T_{01}$ [K]	1800	440
$T_{wall}$ [K]	1200	310
$T_{wall} / T_{01}$	0.67	0.67
$P_{01}$ [bar]	20	1.62
$P_{01} / P_{S3}$	3	3
Mass flow [kg/s]	50	10.84
Platform	Engine	Rig
$T_s$ main stream [K]	1398	330
$P_s$ main stream [bar]	6.42	0.52
Mach main stream	0.85	0.85
$P_{0r}$ coolant [bar]	7.8	Free
$T_{0r}$ coolant [bar]	700	290 – 285
Pratio cooling holes	1.22	Free

**Table 1: Engine-rig mainstream and platform cooling comparison**

The heat transfer process of a real engine is

reproduced in a short duration turbine test rig by a sudden release of hot gas over a cold turbine. A comparison between some relevant main stream features in the test rig and the actual engine configuration is presented in Table 1. The use of research turbines allows reproducing the flow main non-dimensional numbers in a less severe environment. The gas to wall temperature ratio is respected in the experiments, as well as pressure ratios and Mach and Reynolds number levels. Table 1 compares also cooled rotor platform data in the engine and the rig. While the main stream to coolant pressure ratios encountered in actual film cooling schemes are easily matched, generally the target temperature ratio is more difficult to accomplish experimentally since very low coolant temperatures are required.

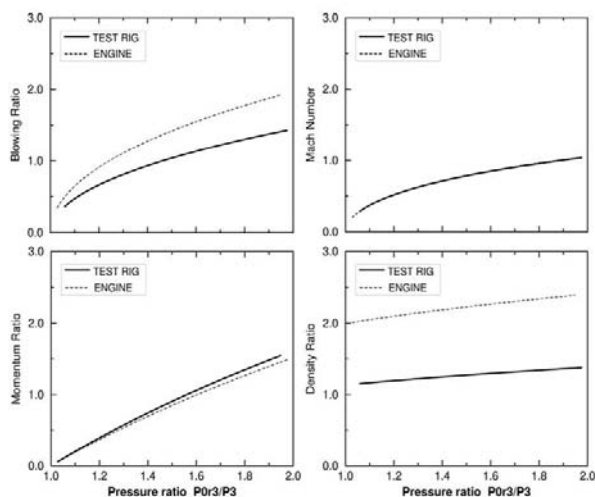


**Figure 1: Film cooling parameters, comparison rig-engine**

Figure 1 shows the evolution of the different film cooling parameters as a function of the pressure ratio across the holes for the rig configuration and engine conditions. The cooling parameters are defined as follow:

$$Dr = \frac{\rho_c}{\rho_f}; Br = \frac{\rho_c V_c}{\rho_f V_f}; Mr = \frac{\rho_c V_c^2}{\rho_f V_f^2} \quad (1)$$

Where  $\rho_c, V_c$  refers respectively to the coolant density and velocity while  $\rho_f, V_f$  to the correspondent main stream variables.

The blowing ratio can be easily varied in order to match the engine configuration. However the rig density ratio is far from the actual density ratio encountered in actual film cooling practice. To match the density ratio expensive cryogenic techniques are required, otherwise a denser gas can be used as alternative solution.

### 3.2. Transonic turbine

The tests were performed in a full high-pressure transonic turbine stage operating under engine-representative conditions. Figure 2 displays the current turbine stage, together with a meridional cut showing the path of the coolant to the wheelspace cavity and the rotor platform. The nozzle guide vane is composed of 43 front-loaded vanes, designed to operate in the transonic regime (Sieverding et al., 1996). Therefore, the vane to vane channel is convergent with a flat rear suction side. The rotor is made-up of 64 highly loaded transonic rotor blades. The highly loaded blades are designed with an inlet metal angle of about 45 deg. and a turning of about 105 deg. to limit the secondary flows. Negative blade lean further reduces secondary flows in the tip region.

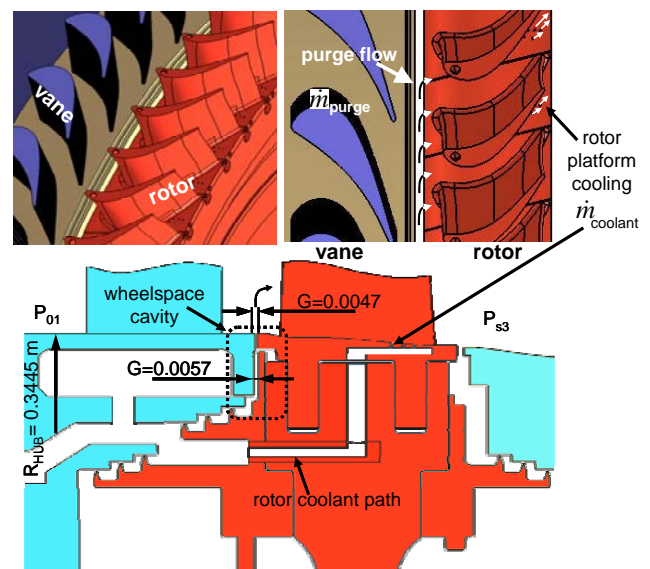


**Figure 2: Turbine stage and platform coolant path**

### 3.3. Cooling system

The platform cooling is applied to a sector of 17 contiguous blades. The coolant comes out of the platform through five cylindrical holes inclined at 30 deg. and located in the platform region close to the rotor blade rear suction side. The stator-rim purge flow coolant is injected radially towards the main channel, as shown in Figure 2. Significant changes to the previous experimental apparatus were implemented to meet the experimental objectives. In particular two heat exchangers and a pre-swirler were added to the existing hardware, as shown in Figure 3.

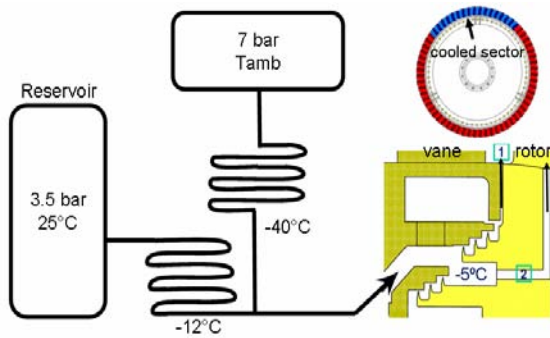


Figure 3: Turbine platform cooling scheme

Well in advance performing a blow-down test, all the coolant path from the reservoir to the rotor is cooled down by means of a secondary heat exchanger operating at  $-60^{\circ}\text{C}$  (Carbo-ice and Methanol). Once the temperature is satisfactory, the main reservoir is vented through a major heat exchanger ( $-20^{\circ}\text{C}$ ) allowing the required massflow rates. Before entering the rotor disk, the coolant air passes through a pre-swirler with an exit angle of  $80^{\circ}\text{C}$  (Figure 4). By swirling the flow at the rotor inlet, the total relative coolant temperature is kept low, up to 10 degrees lower with respect to the axial injection. The coolant air finally reaches the rotor disk cavity, where part of it is injected into the rotor (location 2), feeding the platform cooling holes, and the rest leaks through the labyrinth seals producing the hub disk leakage flow (location 1).

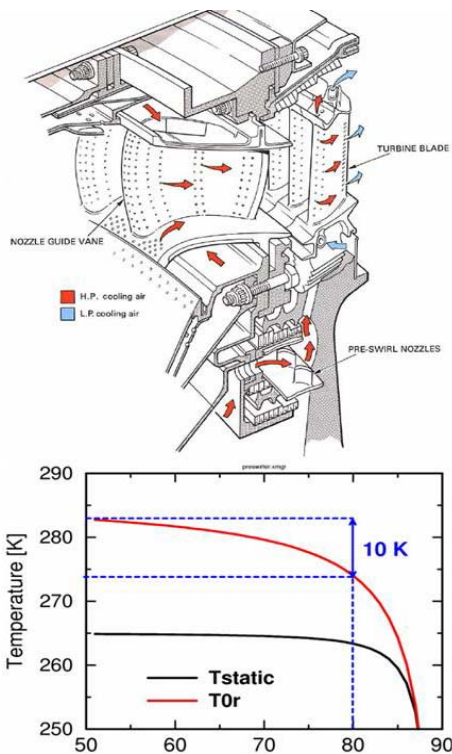


Figure 4: Pre-swirler 3D view and operating point at design conditions (figure extracted from The Jet Engine by Rolls Royce plc., 1996)

### 3.4. Instrumentation

Capturing properly the aero-thermal impact of film cooling and inter-stage purge flow ejection in such an environment requires a significant effort in terms of instrumentation. Global quantities have been measured at three different locations along the turbine axis as depicted in Figure 5. Radial traverses of pressure and temperature have been performed upstream (plane 1) and downstream (plane 3) of the turbine stage using Kiel probes, static pressure taps and miniaturized type K thermocouples.

The static pressure at the vane exit (plane 2) ( $0.035x C_{ax}$ ) is measured at 10 locations along the hub endwall, covering one stator pitch. The rotor-stator annular gap is instrumented on the stator rim with 10 pressure tappings distributed over one vane pitch. Both pneumatic taps and sub-surface mounted fast response transducers have been used. Thin film gauge resistors mounted on an insulating substrate (Upilex) around the airfoil measure the heat transfer rates to turbine blades (Schultz and Jones, 1973). On the cooled rotor platform, due to the strong temperature gradients inside the metal, a second boundary condition is necessary to retrieve the heat flux, so that foil thermocouples have been placed underneath the gauges. The rotor blade static pressure has been measured at 15% of the blade height and platform surface with high frequency response pressure sensors.

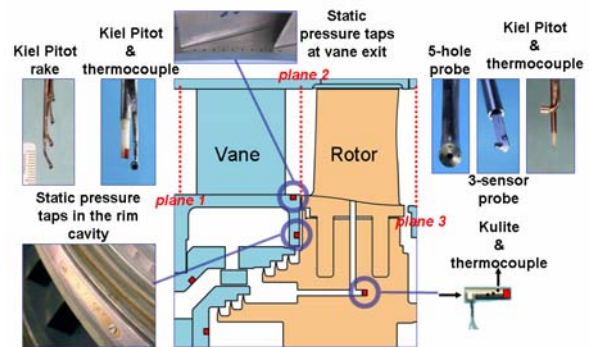
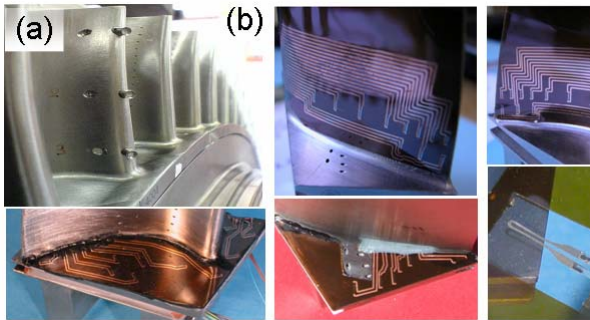


Figure 5: Meridional view of the turbine, measurements planes and instrumentation

The stagnation pressure at the rotor leading edge (15%, 50% and 85%) has been obtained with recessed Pitot probes as depicted in Figure 6. Since the rotor incidence angle changes at high frequency, the shield placed around the sensors allows retrieving accurately the stagnation pressure in the relative frame. The fast response instrumentation mounted on the rotor blades should ensure a frequency bandwidth above 30 kHz to

resolve the large vane passing pulsations (at 4.7 kHz) and its harmonics.



**Figure 6: a) Rotor blade leading edge instrumentation b) Heat transfer instrumentation**

### 3.5. Data processing techniques

In high speed flows (in the transonic and supersonic regimes), the local adiabatic wall temperature  $T_{aw}$  is more appropriate than the local gas temperature to obtain a convective heat transfer coefficient independent from the thermal boundary condition of the specific test (Popp et al., 1999). The heat transfer coefficient becomes a function of the geometry, flow field and fluid properties, allowing decoupling effectively the individual effects of the flow field and of the temperature difference:

$$h_{aw} = \frac{\dot{Q}}{(T_{aw} - T_w)} \quad (2)$$

The temperature oscillations present in the current cooled configuration short testing prevented an accurate fit of the experimental temperature differences with linear laws, to be able to extrapolate the adiabatic wall temperature. A close approximation to the adiabatic wall temperature is the recovery temperature which can be calculated as follows:

$$T_{recovery} = T_s + r(T_0 - T_s) \quad (3)$$

$$T_0 = \left(1 + \frac{\gamma - 1}{2} \cdot M^2\right) \cdot T_s \quad (4)$$

where the isentropic Mach number  $M$  is based on the measured upstream total pressure and the measured static pressure on the rotor blade. A turbulent recovery factor  $Pr^{1/3} = 0.89$  was assumed (Schlichting and Gertsen, 1965). This choice of the recovery temperature ensures that  $h$  and  $Nu$  are reasonably independent of the thermal boundary condition. This approach has been extensively used in the literature (Thorpe et al, 2004).

The Nusselt number presented in all the plots is a scaled heat flux, as it is defined in terms

of the airfoil axial chord, total inlet temperature minus the local profile temperature, and thermal conductivity based on the local temperature. 2D heat conduction computations have been performed to obtain the initial flux due to the preheating caused by the prerotation prior to the actual blow down (Solano et al., 2008). The experimental wall temperature time evolution during the pre-rotation process has been used as a boundary condition. Two dimensional effects are seen to be significant at the leading and trailing edges. It has been proved that the actual heat flux during a test can be calculated by superposition of the initial flux preheating and the actual flux during the blow down. The overall uncertainty on the Nusselt number was evaluated to be  $\pm 7.5\%$ .

Measuring the unsteady pressure fluctuations requires the use of dedicated transducers with a low membrane inertia which is directly in contact with the flow. All high-speed pressure transducers used in this measurement campaign are manufactured by Kulite Semiconductor Inc., a leading company in the field of pressure measurement technology. The transducers are made out of a thin silicon diaphragm, on the surface of which piezoresistors are manufactured by photolithographic techniques and diffusion of doping atoms either of the first or fifth atomic group. Typically four elongated piezoresistors are formed on the membrane, and are positioned in such a way that, when pressure is applied on the sensor, two of them are put under compressive strain and the other two under tensile strain. They are then interconnected to form a Wheatstone bridge of overall constant resistance. Figure 7 shows a photo and an illustration of such a silicon membrane. When a piezoresistor is strained, its resistance changes and moves the bridge off-balance. At constant temperature, the measurement of the bridge imbalance is directly proportional to the pressure applied on the silicon membrane.

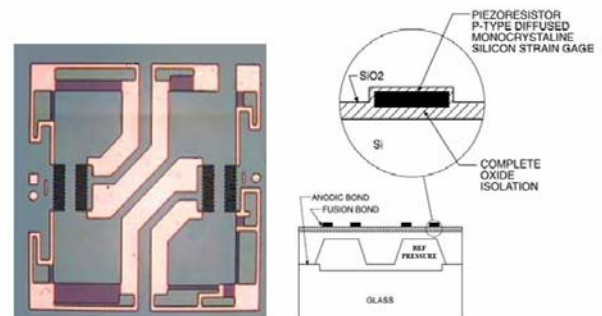


**Figure 7: Picture and schematics of a silicon diaphragm**

In the VKI compression tube facility CT3, temperature variations during the blowdown are induced by several factors:

- The compression of the gas in the tube before the blowdown increases the temperature of the air to values in excess of 430 K (as recorded close to and upstream of the guide vane).
- When the air comes in contact with the cold metal of the test section (the vane, the rotor and the endwalls), heat transfer occurs.
- Windage losses increase the temperature of the rotor blades during the run-up prior to the test.
- The expansion of the gas in both the guide vane and the rotor decreases its temperature.

Because of the sensitivity of the resistance of the piezoresistors to temperature, the actual circuitry of the bridge is modified, to account for temperature compensation. Among the different techniques used to compensate for temperature dependency, two main groups can be identified: passive and active compensation. In passive compensation, the typical approach is to add external resistors in series with the bridge, to reduce the sensitivity of the bridge output to thermal influence, at the expense of a lower signal-to-noise ratio. This technique has been made available by the manufacturers since the beginning of the piezoresistive sensor technology. In active compensation, the overall bridge resistance, which reflects the sensors temperature, is taken into account and used to correct the pressure signal output by the bridge. This can be done using more circuitry to modify the bridge output, or through post-test numerical correction. The post-processing technique is used at the VKI because it is best suited to the treatment of temperature transients. If temperature compensation is not applied a numerical analysis shows that an increase in temperature results in a decrease in the offset, an increase in the slope, and overall an underestimation of the true pressure (Dénos and Valenti, 2000).

### 3.6. Operation of the facility

Prior to a blow-down test, the entire coolant path is refrigerated by means of a secondary cooling circuit operating at  $\sim 213$  K.

During the actual blow-down the main heat exchanger cools down all the coolant flows, venting the flow into the wheelspace and rotor channels at  $\sim 280$  K. Pressure and temperature sensors located along the whole flow path allow calculating the coolant mass flow rates through the injection channel elbow, the wheelspace cavity, and the rotor platform cooling channel.

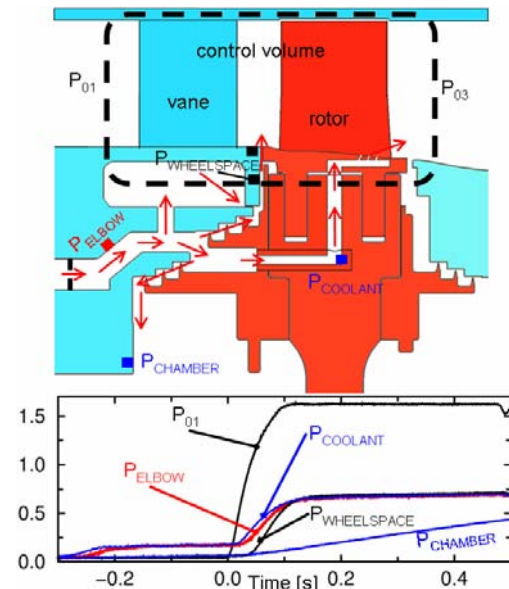


**Figure 8: Coolant flow paths and pressure transients during a typical test**

Figure 8-top depicts the path followed by the coolant from the entrance to the test section through twelve elbow pipes to the three possible outlets: the internal chamber; the rotor platform film cooling; or ejection into the wheelspace. For completeness, pressure sensors in the wheelspace cavity serve to monitor the regions where there is net flow ingress or flow ejection.

Figure 8-bottom shows pressure traces at different locations in the coolant path together with the evolution of the stage total inlet pressure  $P_{01}$  during the actual testing time ( $\sim 0.4$  s). The coolant injection starts 0.35 seconds before the actual blow down to allow the coolant flow to reach steady state. Once the desired blowing ratios are established, the high pressure and temperature mainstream gas is blown into the stage, producing the sudden increase in  $P_{01}$ . The pressure rise in the mainstream channel pressurizes all the inner cavities, remaining constant afterwards during the blow down time. As the measured traces reach a steady regime, in a temporal window confined between  $t = 0.15$  s and  $t = 0.2$  s, all the measured values are time averaged. This averaging procedure allows to retrieve pressure and temperature values representative of a full steady state condition for

each test.

The test ends at  $t = 0.4$  s when the upstream total pressure  $P_{01}$  drops either because the piston reaches the end of its stroke or because the sonic throat becomes unchoked. Finally, the rotor is slowed down using an aero brake.

## 4. Results

### 4.1. Test conditions

The different conditions have been designed in order to operate at platform blowing ratios below 1.35 and sufficiently high to avoid hot gas ingestion into the cavities. Table 3.1 summarizes the test conditions, indicating the amount of coolant injected through the rotor platform and hub cavity as a percentage of the main stream mass flow.

Condition	$\dot{m}_{\text{purge}}$ [%]	$\dot{m}_{\text{coolant}}$ [%]	$Br$	$Dr$	$Mr$
Ingestion - 1 %	-1.00	0.020	0.59	1.14	0.32
Ingestion - 0.2 %	-0.18	0.034	1.09	1.38	0.93
Ejection +0.3 %	0.28	0.043	1.16	1.38	1.32
Ejection +0.8 %	0.76	0.040	1.01	1.34	1.2
low-RPM	0.15	0.038	1.35	1.33	1.01

Table 2: Film cooling parameters for the different test conditions

In the baseline condition, “ingestion -1%” there is no coolant injection, but there is nevertheless gas exiting the cooling holes at a rate of 0.02 %, while ingestion of air inside the large inner cavity (which is initially at vacuum) leads to ingress of the mainstream flow of -1 % through the disk cavity. In the “ingestion -0.2%” condition, coolant is injected in the facility. The mass flow through the platform is increased by 70 % leading to a blowing ratio of 1.09. The ingestion at the stator-rotor interface is reduced to -0.18 % due to higher pressurization of the annular chamber in between the labyrinths. The amount of coolant injected in the facility increases by 50% from “ingestion -0.2%” condition to “ejection +0.3%”, leading to a further increase of the mass flow rate traversing the platform at a blowing rate of 1.35 and a net ejection of air at the hub disc cavity of +0.28%. Keeping the same amount of injection as in, but lowering the RPM to 4700 reduces the amount of gas coming out of both the rotor platform (blowing rate 1.16) and the hub disc

cavity: +0.15% .This is due to the greater seal clearance which allows more air to go into the core chamber and the different pressure distribution. Finally, in the “ejection+0.8%” condition, a new pathway is opened to the hub disc cavity (through the outer casing of the pre-swirler).This allows increasing the net amount of air ejected at the stator-rotor interface , reaching +0.76 %, while keeping the platform blowing rate low: 1.01.

### 4.2. Coolant Flow Temperature

The coolant temperature statistics in the rotor coolant channel measured by mean of a thermocouple in rotation is presented in Table 3. Note that is a relative temperature and therefore values are higher than the coolant temperature in the stationary frame.

Condition	Coolant Temperature [K]	$1.98 \sigma$ [K]
Ingestion - 1 %	299	1.3
Ingestion - 0.2 %	299	1.3
Ejection +0.3 %	291	5.6
Ejection +0.8 %	288	6.3
low-RPM	295	4.7

Table 3: Statistics coolant temperature measured in rotation

Figure 9 shows the time evolution of the coolant temperature measured in the rotating frame for different tests covering all operating conditions. The data shows a pronounced scattering on the actual initial temperature before any coolant injection takes place (i.e. time < 0.5s). That initial temperature depends on different factors: the atmospheric temperature, number of runs of the day, pre-rotation time, vacuum level on the test section during pre-rotation time, and it is therefore very difficult to control or repeat from test to test. At time  $\sim -0.4$ s a small overshoot occurs followed by a decrease in the measured temperature, corresponding to the start of the injection. The sudden pressurization of the coolant channels produces the overshoot, while the temperature thereafter decreases constantly due to the cold flow going through the channels. The blow down takes place at time  $\sim 0$ s. The main-stream flow pressurizes all the cavities and coolant channels, producing this time a stronger overshoot, followed again by a slight decrease in temperature.

The absolute coolant temperature during a

test does depend significantly on the actual temperature of the rotor before the injection takes place. The small amount of air flowing through the coolant channels is not able to cool down the massive metallic components in its pathway towards the rotor platform. Figure 9 visualizes also a total inlet pressure trace P01, shown as reference, which gives information on the actual test duration.

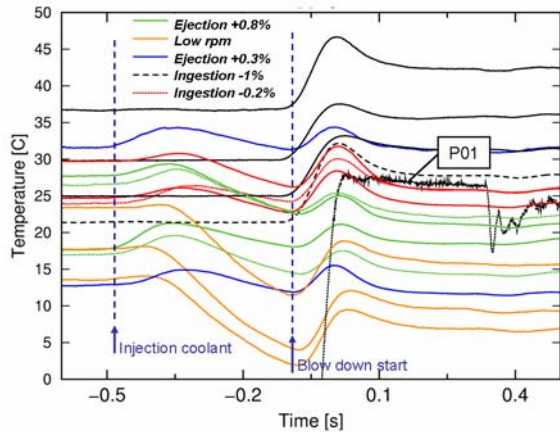


Figure 9: Coolant temperature traces during the blow down time

Even though the coolant temperature absolute value is not very repeatable from test to test, its time evolution is repeatable as depicted in Figure 10.

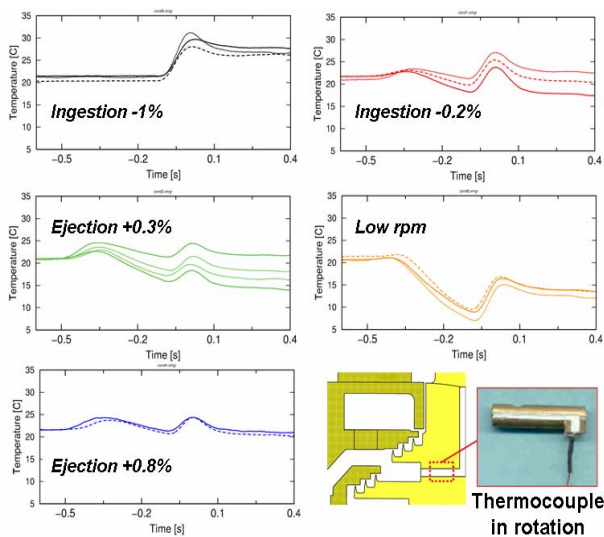


Figure 10: Coolant temperature traces in the rotating frame

Note that the traces have been all shifted to the same initial value for clarity. At condition “ingestion -1%”, the lack of injection results in only one overshoot corresponding to the start of the blow down. Besides, there is a net temperature increase due to the hot mainstream gas entering the

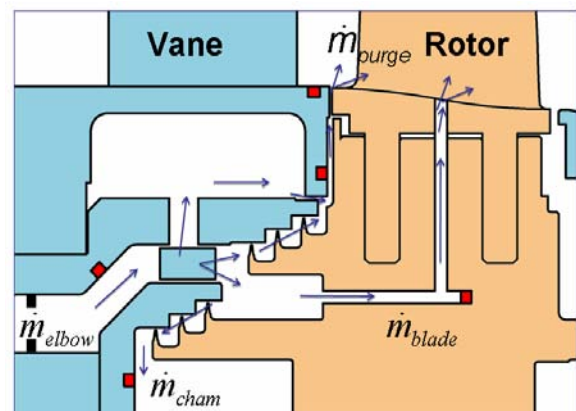
rotor coolant channel of about 6 to 7 degrees. At conditions “ingestion -0.2%”, “ejection +0.3%” and “ejection +0.8%” the traces present similar trends, with smooth temperature decay rates. Condition “low rpm”, presents a high decrease of temperature right after the injection. That is due to the combination of two effects: reducing the rotational speed (4700 rpm), the pre-rotation time needed is shorter allowing a colder rotor temperature and therefore less heating. On the other hand the coolant relative inlet temperature is smaller since the peripheral speed is smaller too.

### 4.3. Coolant mass flows

The absolute amount of coolant injected in the facility ( $\dot{m}_{elbow}$ ) is controlled by means of sonic holes which remain choked during the test. Figure 11 illustrates the coolant mass flow measured, with the corresponding uncertainty level evaluated. The pressure is monitored on both sides of the sonic hole. Measuring additionally the absolute temperature upstream allows the computation of the mass flow rate through the hole by using the following equation:

$$\dot{m}_{elbow} = 0.0404 \cdot C_d \cdot S \cdot \frac{P}{\sqrt{T}} \quad (5)$$

where  $C_d$  is the discharge coefficient.



Condition	$\dot{m}_{elbow}$ [%]	$\dot{m}_{cham}$ [%]	$\dot{m}_{purge}$ [%]	$\dot{m}_{blade}$ [%]
	$\pm 0.025$	$\pm 0.007$	$\pm 0.04$	$\pm 0.004$
Ingestion - 1 %	0	0.98	-1.00	0.020
Ingestion - 0.2 %	1.03	1.18	-0.18	0.034
Ejection +0.3 %	1.52	1.197	0.28	0.043
Ejection +0.8 %	1.51	0.71	0.76	0.040
Low-RPM	1.99	1.80	0.15	0.038

Figure 11: Coolant mass flow measured

The mass flow leaking towards the inner chamber can be easily calculated since the volume of the chamber is known and the pressure and temperature time evolution in the chamber are recorded. The mass flow is retrieved by calculating the time derivative of density:

$$\dot{m}_{chamber} = \frac{d}{dt}(\rho V)_{chamber} \quad (6)$$

The amount of coolant traversing the blades is calculated with a model. The inputs to the model are the pressure inside the blade and the mainstream platform static pressure. An experimentally measured variable discharge coefficient has been also obtained at VKI for the film cooling holes.

The mass flow through the cooled blades is determined thanks to the knowledge of the pressure inside the rotor coolant supply channels (measured), the static pressure in the test section at the holes exit (from a 3D Navier-Stokes computation), the geometrical characteristics of the holes and the discharge coefficient determined experimentally for different pressure ratios.

The total to static pressure ratio allows computing the Mach number. With the total temperature, the isentropic velocity across each hole can be computed and thus the isentropic mass flow. The real mass flow is the product of the isentropic mass flow times the discharge coefficient.

Given the uncertainties of each quantity involved in the computation of the mass flow, one can derive the corresponding uncertainty of the efficiency using the equation (7).

$$\Delta m = \sqrt{\sum_{i=1}^n \left( \frac{\partial m}{\partial x_i} \Delta x_i \right)^2} \quad (7)$$

Where  $x_i$  corresponds to the quantities involved in each mass flow computations. Given the complexity of the analytical formulation, it would be not realistic to start expanding the derivatives of the mass flow with respect to all input quantities analytically. The derivative can be approximated according to equation (8). In this equation,  $\Delta x_i$  is the uncertainty of the quantity  $x_i$  and  $\Delta m_i$  is the change of mass flow caused by a variation  $\Delta x_i$  on  $x_i$ . The only assumption involves that the uncertainty of each quantity and the derivative do not dramatically vary for such a small change.

$$\frac{\partial m}{\partial x_i} = \frac{\Delta m}{\Delta x_i} \quad (8)$$

As result, equation (7) can be approximated using equation (8). Thus the entire process consists of three steps: (1) computation of the efficiency with all nominal value; (2) successively computation of the changes of efficiency when a single quantity is varied, by its uncertainty; (3) summation of the squared differences and computation of the square root.

$$\Delta m = \sqrt{\sum_{i=1}^n (\Delta m_i)^2} \quad (9)$$

Beside deriving the uncertainty associated to the derived mass flows, the sensitivity to each value are illustrated to indicate the relative change in the mass flow due to the uncertainty of each single quantity. Table 4 illustrates uncertainty and sensitivity analysis for the measured purge mass flow.

Quantity	Unit	Mean value	Uncertainty	Sensitivity	Mass Flow Change [kg/s]
Pcham	[bar]	0,280	0,01	0,01	0,0002
Tcham	[K]	310,8	2	1,32	0,0070
Pinj1	[bar]	5,512	0,015	1,38	0,0031
Tinj1	[K]	270,5	3	-0,69	-0,0063
Pinj2	[bar]	5,233	0,015	9,87	0,0234
Tinj2	[K]	279,5	3	-0,48	-0,0043
Pcool2	[bar]	0,846	0,01	-0,06	-0,0006
Tcool2	[K]	286,7	3	0,03	0,0003
		Quantity	Mean [kg/s]	Uncertainty	
		M purge	0,827	0,0258	

Table 4: Uncertainty and sensitivity analysis

## 5. Efficiency measurements

The efficiency was evaluated considering the mechanical approach, in which the real power is retrieved from the measurement of the shaft power, based on the measurement of the inertia (Paniagua and Yasa, 2007) and mechanical losses. The power can thus be expressed:

$$P_{real} = P_{shaft} + P_{losses} = I \omega \frac{\partial \omega}{\partial t} + P_{loss} \quad (10)$$

Where  $P_{loss}$  accounts for the mechanical losses. The control volume used to evaluate efficiency is shown in Figure 8. The inlet and outlet planes of the control volume coincides with the measurements planes. The purge flow temperature and pressure were monitored with a thermocouple and a pressure transducer on the rotor disc coolant path. This allows gathering the total temperature and pressure levels of the coolant injected. Hence the isentropic power can be expressed as follow:

$$P_{is} = \dot{m}_{inlet} C_p T_{01} \left[ 1 - \left( \frac{P_{03}}{P_{01}} \right)^{\frac{\gamma-1}{\gamma}} \right] + \dot{m}_{coolant} C_p T_{0coolant} \left[ 1 - \left( \frac{P_{03}}{P_{0coolant}} \right)^{\frac{\gamma-1}{\gamma}} \right] \quad (7)$$

Due to the variation of inlet and total pressure variables along the span, the efficiency formulation makes use of mass flow average quantities. Due to the complexity and size of the facility, it is difficult to install a standard metering system such as a Venturi or orifice plates. Monitoring the location of the piston, the total pressure and the total temperature it is possible to know the mass of air downstream of the piston at any time and hence the massflow:

$$\dot{m} = \frac{d\rho \cdot V}{dt} = \frac{P_{0tube}}{\mathfrak{R} \cdot T_{0tube}} \frac{dV}{dt} = \frac{P_{0tube}}{\mathfrak{R} \cdot T_{0tube}} \frac{dV}{dt} \frac{\pi D^2}{4} \frac{dx}{dt} \quad (8)$$

To estimate all the quantities, a 0-dimensional model performs balances of mass flow and energy as a function of time in the different volumes of the rig, i.e. the upstream tube, the settling chamber and the downstream dump tank (Denos et al., 2006). This procedure requires the measurement of the upstream total pressure  $P_{01}$ , total temperature  $T_{01}$ , the estimation of the sonic throat area  $A$ , and the discharge coefficient  $C_d$ . In order to take into account possible differences between the tube exit and the stage inlet, which are separated by a settling chamber, the turbine is assimilated to a sonic orifice. The mass flow can thus be computed according to:

$$\dot{m} = C_d \frac{P_{01}}{\sqrt{C_p T_{01}}} A \frac{\gamma}{\sqrt{\gamma-1}} \left[ \frac{\gamma+1}{2} \right]^{\frac{-(\gamma+1)}{2(\gamma-1)}} \quad (5)$$

Once the model is fitted to an ensemble of tests, a virtual test is run under perfectly constant conditions. The mass flow conservation between the tube exit and the stage inlet can be applied and the coefficients determined. Table 5 summarizes the inlet mass flows evaluated according to this procedure.

Condition	$\dot{m}_{INLET}$ [kg/s]	$\dot{m}_{OUTLET}$ [kg/s]	$\pm 1.96 \sigma$
<i>ingestion -1 %</i>	9.94	9.84	0.073
<i>ejection +0.3 %</i>	9.91	9.94	0.109
<i>ejection +0.8 %</i>	9.88	9.96	0.104
<i>Low-RPM</i>	9.88	9.90	0.103

**Table 5: Turbine mass flow measured**

The outlet mass flows were obtained adding or subtracting the purge flow and rotor platform coolant. Negligible differences are appreciated on the turbine inlet mass flow, the

dispersion remains within the random error estimated by statistical analysis to be  $\pm 0.1$  kg/s. Finally the efficiency can finally been expressed as the ratio between the real and isentropic power:

$$\eta = \frac{I\omega \frac{\partial \omega}{\partial t} + P_{loss}}{(\dot{m}_{inlet} - \dot{m}_{leakage}) C_p T_{01} \left[ 1 - \left( \frac{\bar{P}_{03}}{P_{01}} \right)^{\frac{\gamma-1}{\gamma}} \right] + \dot{m}_{coolant} C_p T_{0coolant} \left[ 1 - \left( \frac{\bar{P}_{03}}{P_{0coolant}} \right)^{\frac{\gamma-1}{\gamma}} \right]} \quad (9)$$

The leakage mass flow refers to hot gas ingestion from the main channel into the wheelspace cavity and therefore appears only in the baseline condition. The coolant mass flow is the cold flow purged from the wheelspace and rotor platform. The measured efficiency are illustrated in Table 6.

Condition	$\eta$ [%]	$\Delta\eta$ [%]	$\pm 1.96 \sigma$ [%]
<i>Ingestion -1%</i>	92.47	0.00	1.81
<i>Ejection +0.3%</i>	93.39	0.92	1.79
<i>Low rpm</i>	82.82	-9.65	1.92
<i>Ejection +0.8%</i>	93.25	0.78	1.95

**Table 6: Measured turbine efficiency**

The level of dispersion in the measured efficiency is almost 1.9 % ( $\pm 1.96\sigma$ ). The reason for such low repeatability in the efficiency measurements are mainly related to dispersion in the turbine mass flow measurements. Moreover dispersion on the total pressure measurements downstream of the rotor contributes to decrease the repeatability in the efficiency measurements. Table 6 summarizes the measured turbine efficiency variations for the different test conditions evaluated considering the baseline (*ingestion -1 %*) as reference. At *ejection +0.3 %* the efficiency is +1.11% higher, but when the massflow is further raised to *ejection +0.8 %* the efficiency is +1.04% above the baseline. Measurements show the same trend: injecting purge flow leads to an increase in efficiency, which might be due to the modification of the shock system downstream of the stator and to a reduction of the stator trailing edge shock losses.

## 6. Conclusions

Hub disk leakage and hub rotor platform film cooling experiments have been carried out in a fully rotating HP transonic turbine stage under engine representative conditions. Several test conditions have been tested in order to analyze

independently the effects of the rotor platform cooling, the hub disk leakage, and the rotational speed.

The turbine test rig has been modified in order to provide the required coolant flow rates and temperatures. Two heat exchangers have been used to cool down the flow injected in the turbine. Hub disk leakage coolant flow injection from the stator-rotor rim cavity contributes to a blockage effect which results in a lower transonic loading of the turbine, with reduced Mach numbers at the stator outlet and with increased pressure ratio across the vane row. Turbine mass flow and turbine efficiency have been measured, and despite a relevant dispersion in the efficiency repeatability, a clear trend was observed in increasing turbine efficiency when injecting coolant flow from the wheel space disk cavity. A more detailed efficiency analysis on the loss breakdown, objective of future research, will help to explain the causes of this change in the turbine efficiency.

## 7. Acknowledgments

The authors would like to acknowledge Bertrand Haguenaer and Tolga Yasa for their assistance in the testing. The authors would also like to acknowledge the financial support of the European Commission and Industrial Partners involved in TATEF2 "Turbine Aero-Thermal External Flows 2".

## 8. References

- Abhari, R.S., and Epstein, A.H., 1994, "An Experimental Study of Film Cooling in a Rotating Transonic Turbine," *ASME J. of Turbomachinery*, 116, pp. 63-70.
- Ahn, J., Schobeiri, M.T., Han, J.C., and Moon, H.K., 2004, "Film Cooling Effectiveness on the Leading Edge of a Rotating Turbine Blade," *IMECE 2004-59852*.
- Anker, J.E., Mayer, J.F., 2002, Simulation of the Interaction of Labyrinth Seal Leakage Flow and Main Flow in an Axial Turbine, *ASME Paper*, GT2002-30348.
- Blair, M.F., 1974, "An Experimental Study of Heat Transfer and Film Cooling on Large-Scale Turbine Endwalls," *ASME J. of Heat Transfer*, pp. 524-529.
- Blair, M.F., 1994, "An Experimental Study of Heat Transfer in a Large-Scale Turbine Rotor Passage," *ASME J. of Turbomachinery*, 116, pp. 1-13.
- Bohn, D., Deuker, E., Emunds, R., and Gorzelitz, V., 1995, "Experimental and Theoretical Investigations of Heat Transfer in Closed Gas-Filled Rotating Annuli", *ASME J. Turbomach.*, 117, pp. 175-183.
- Cao, C., Chew, J. W., Millington, P. R., and Hogg, S. I., 2003, "Interaction of Rim Seal and Annulus Flows in an Axial Flow Turbine," *ASME paper no. GT2003-38368*.
- Dénos R., Paniagua G., Yasa T., Fortugno E., 2006, "Determination of The Efficiency of a Cooled HP Turbine in a Blowdown Facility", *ASME Paper*, GT2006-90460.
- Dénos, R. and Paniagua, G., 2005: "Rotor/Stator interaction in Transonic HP Turbines". VKI Lecture Series on "Effects of Aerodynamic Unsteadiness in Axial Turbomachines". VKI LS 2005-03. ISBN: 2-930389-59-1. Sint Genesius Rode.
- Dring, R. P., Blair, M. F., and Hoslyn, H. D., 1980, "An Experimental Investigation of Film Cooling on a Turbine Rotor Blade", *ASME J. of Engineering for Power*, 102, pp. 81-87.
- Friedrichs, S., Hodson, H.P., Dawes, W.N., 1996, "Distribution of Film-Cooling Effectiveness on a Turbine Endwall Measured Using Ammonia and Diazo Technique," *ASME J. of Turbomachinery*, 118, pp.613-621.
- Gentilhomme, O., Hills, N. J., Turner, A. B., and Chew, J. W., 2003, "Measurement and Analysis of Ingestion Through a Turbine Rim Seal," *ASME J. Turbomach.*, 125~3!, pp. 505-512.
- Harasgama, S.P., and Burton, C.D., 1992, "Film Cooling Research on the Endwall of a Turbine Nozzle Guide Vane in a Short Duration Annular Cascade: Part 1 - Experimental Technique and Results," *ASME J. of Turbomachinery*, 114, pp.734-740.
- Hunter, S. D., and Manwaring, S. R., 2000, "Endwall Cavity Flow Effects on Gaspath Aerodynamics in an Axial Flow Turbine: Part 1: Experimental and Numerical Investigation," *ASME paper no. 2000-GT-651*.
- Ko, S. H., and Rhode, D. L., 1992, "Thermal Details in a Rotor-Stator Cavity at Engine Conditions With a Mainstream," *ASME J. Turbomach.*, 114, pp. 446-453.
- Laroche, E., Desportes de la Fosse, S., Djaoui, M., Debuchy, R., and Pate', L., 1999, "A Combined Experimental and Numerical Investigation of the Flow in a Heated Rotor/Stator Cavity With a Centripetal Injection," *ASME paper no. 99-GT-170*.

Marini R., Girgis S., 2007: "The effect of blade leading edge platform shape on upstream disk cavity to mainstream flow interaction of a high-pressure turbine stage". ASME Paper 2007-27429.

McLean, C., Camci, G., and Glezer, B., 2001, "Mainstream Aerodynamic Effects due to Wheel-space Coolant Injection in a High Pressure Turbine Stage. Part 1: Aerodynamic Measurements in the Stationary Frame. Part 2: Aerodynamic Measurements in the Rotational Frame", ASME J. Turbomach., 123~4!, pp. 687–696 and 697–703.

Ong J.H.P., Miller R.J., and Uchida S., 2006: "The effect of coolant injection on the endwall flow of high-pressure turbine". ASME Paper GT2006-91060.

Paniagua, G., Denos, R., Almeida, S., 2004, "Effect of the Hub Endwall Cavity Flow on the Flow Field of a Transonic High-Pressure turbine," ASME J. of Turbomachinery, 126, pp. 578-586.

Paniagua, G., and Yasa, T., 2007 "Accurate turbine inertia measurement". *J. Experimental Mechanics*, 47, pp 693-700.

Pfau, A., Treiber, M., Sell, M., Gyarmathy, G., 2001, Flow Interaction From the Exit Cavity of an Axial Turbine Blade Row Labyrinth Seal, Transaction of the ASME, Journal of Turbomachinery, Vol. 123, pp. 342-352, April 2001.

Phadke, U. P., and Owen, J. M., 1988, "Aerodynamic Aspects of the Sealing of Gas-Turbine Rotor-Stator Systems" *Int. J. Heat Fluid Flow*, 9 2, pp. 98–117.

Popp O., Smith D., Bubb J., Grabowski H., Diller T., 1999, "Steady and Unsteady heat transfer in a transonic Film Cooled Turbine Cascade". ASME 99-GT259.

Rosic, B., Denton, J. D., 2006, The Control of Shroud Leakage Loss by Reducing Circumferential Mixing, ASME Paper GT2006-90946.

Roy, R. P., Xu, G., Feng, J., and Kang, S., 2001, "Pressure Field and Main-Stream Gas Ingestion in a Rotor-Stator Disk Cavity," ASME Paper no. 2001-GT-0564.

Schlichting, H., and Gertsens, K., 1965, "Boundary layer theory", Ed. Springer, Berlin.  
Sieverding C.H., Arts T., Dénos R. and Martelli F., 1996: "Investigation of the Flow Field Downstream of a Turbine Trailing Edge Cooled Nozzle Guide Vane". *Journal of Turbomachinery*. April, Vol. 118, No. 2, pp 291-300.

Solano J.P., Paniagua G., de la Loma A., 2008: "Novel 2D unsteady heat conduction

calculation in a cooled rotor: Ventilation preheating – Blowdown flux". To be presented at the ASME Turbo Expo 2008. ASME Paper GT2008- 51308. Berlin, Germany. June.

Takeishi, M., Aoki, S., Sato, T., and Tsukagoshi, K., 1992, "Film Cooling on a Gas Turbine Rotor Blade," ASME J. of Turbomachinery, 114, pp. 828-834.

Thorpe, J., Yoshino, S., Ainsworth, R., Harvey, N., 2004: "Improved Fast Response Instrumentation for Short-Duration Wind Tunnels", *Measurements Science and Tecnology*, Vol. 15, pp 1897-1909.